

Experimental engineering of Floquet topological phases in a one-dimensional optical lattice

Pengju Zhao,^{1,2,3} Yudong Wei,^{1,4,*} Zhongshu Hu,^{1,4} Shengjie Jin,^{1,4} Xuzong Chen,⁵ and Xiong-jun Liu^{1,4,6,†}

¹*International Center for Quantum Materials, School of Physics, Peking University, Beijing 100871, China*

²*Beijing Aerospace Institute for Metrology and Measurement Technology, Beijing 100076, China*

³*Beijing Key Laboratory of Aerospace Photonic Quantum Precision Measurement and Metrology, Beijing 100076, China*

⁴*Hefei National Laboratory, Hefei 230088, China*

⁵*School of Electronics Engineering and Computer Science, Peking University, Beijing 100871, China*

⁶*International Quantum Academy, Shenzhen 518048, China*

(Dated: March 3, 2026)

Periodic driving enables realization of topological phases without static counterparts. We experimentally realize and detect a one-dimensional anomalous Floquet topological phase in an optical lattice, using multi-frequency control to manipulate the sign configuration of the gap windings (W_0, W_π) associated with the 0 and π quasienergy gaps. We develop a lattice-depth modulation scheme that induces staggered nearest-neighbor s - p orbital couplings and realize a minimal nontrivial Floquet topology under single-tone driving. Introducing a second tone, the relative phase provides a physical control knob that sets the effective coupling signs in the two gaps, such that the corresponding windings can be tuned to add or cancel. Aligned windings yield high-winding phases, whereas opposing windings cancel the net Floquet-band invariant while retaining nontrivial gap indices. We read out (W_0, W_π) with a band-inversion-surface (BIS)-resolved Ramsey protocol assisted by lattice position shaking, which measures relative Floquet phases on the BISs. Controlled quenches further confirm phase-dependent band modifications even at quasimomenta far from resonance. These results establish multi-frequency control with a tunable relative phase as a quantitative route to engineering anomalous Floquet topology, and demonstrate phase-coherent coexistence of distinct drive modalities.

I. INTRODUCTION

Topological phases of quantum matter have become a universal concept across modern physics. Periodic driving provides a controlled route to design such phases, including ones without static counterparts [1–3]. A first theme comprises conventional Floquet topological phases, where the stroboscopic dynamics over one period can be captured by an effective static Floquet Hamiltonian H_F within a high-frequency or rotating-frame description. Correspondingly, these phases obey the standard bulk-edge correspondence, essentially independent of the time dimension [4–12]. A second theme is anomalous Floquet topology, in which Floquet-band invariants alone are insufficient to establish the conventional bulk-edge correspondence. Instead, topology is encoded in the full one-period evolution operator, beyond any static description. In particular, it can be specified gap by gap through the global winding numbers (W_0, W_π) of the 0 and π quasienergy gaps [13–16]. Recent studies further reveal that Floquet engineering of local topological structures can realize unconventional Floquet phases whose boundary physics may not be fully captured by these global windings [17].

Beyond conceptual novelty, anomalous Floquet topology is attractive from an experimental perspective since it ties robust edge transport to quasienergy gaps rather

than to individual Floquet bands [18, 19]. More generally, this gap-resolved characterization can remain predictive even when Floquet-band invariants fail to capture edge transport, and it naturally enables control and readout by probing the 0 and π gaps separately [15, 16]. In particular, photonic platforms have explored this regime extensively, including two-dimensional anomalous Floquet lattices exhibiting chiral edge transport even when all Floquet-band Chern numbers vanish [20–23]. Related one-dimensional implementations have also observed anomalous π modes in driven waveguide arrays [24]. Beyond crystalline settings, engineered geometries provide additional knobs for tailoring anomalous edge transport, as exemplified by dual Sierpinski carpets [25].

Ultracold atoms provide a clean platform for Floquet topological matter, with tunable control of band structure, disorder, and interactions [26, 27]. This flexibility holds promise for extending anomalous Floquet topology beyond the noninteracting limit. Nevertheless, experimental realizations remain scarce [28–31]. To date, two key experiments have directly accessed the gap windings (W_0, W_π). Wintersperger *et al.* [29] implemented an anomalous Floquet phase on a hexagonal lattice based on the step-wise modulation protocol [5] and inferred gap-resolved windings from energy gap measurements and local Hall deflections. Zhang *et al.* [31] realized a driven square Raman lattice and extracted windings from quench dynamics within the band-inversion-surface (BIS) framework [17, 32]. In the latter approach, the corresponding windings can be inferred gap by gap from

* weiyd2017@pku.edu.cn

† xiongjunliu@pku.edu.cn

time-averaged spin textures across the BISs, enabling Floquet phase mapping with multiple BIS loops. Existing cold-atom experiments have largely focused on single-tone driving, where multiple quasienergy gaps are opened via higher-order (multi-photon) processes. Systematic, phase-controlled and multi-frequency schemes for tuning individual gap windings, as well as one-dimensional anomalous Floquet phases, remain underexplored. Meanwhile, recent advances in orbital lattices have demonstrated coherent, resonant s - p hybridization, enabling synthetic gauge flux [33] and selectively controlled topological pumping [34, 35]. Beyond single-particle band engineering, orbital degrees of freedom also suggest emerging routes for tunable interactions beyond the lowest band, highlighting the broader potential of orbital platforms [36, 37].

Here we propose and experimentally realize one-dimensional (1D) Floquet topological phases and achieve phase-tunable control of the gap windings (W_0, W_π) using multi-frequency lattice-depth modulation (LDM). Importantly, due to the opposite parity of the s and p orbitals, LDM naturally generates a first-order *staggered* nearest-neighbor s - p coupling. This staggered coupling provides a *minimal* and direct Floquet route to engineering an effective orbital-ladder Hamiltonian [38–40]. Previous realizations of this type of Hamiltonian typically relied on lattice-position shaking (LPS), where the corresponding effective coupling is dominated by second-order (two-photon) processes and is therefore weaker [33–35]. Further, by introducing two-tone LDM at $(\omega_0, 2\omega_0)$, we simultaneously open and address both the 0 and π quasienergy gaps already at first order, enabling access to both high-winding and vanishing-winding Floquet phases with sizable gaps under full control of the relative drive phase. To directly resolve the topology gap by gap, we implement a BIS-resolved Ramsey protocol that measures the relative phase between the left and right BIS momenta, k_L and k_R , for each gap. A robust π phase contrast between k_L and k_R provides a minimal dynamical hallmark of a nontrivial winding in the corresponding gap.

The remainder of the paper is organized as follows. Sec. II develops the effective stroboscopic Hamiltonian relevant to the experiment and details the single-tone preparation and readout protocols, showing that LDM yields a nontrivial effective coupling between s - p orbitals and that LPS and LDM can coherently coexist within a single sequence. Sec. III introduces direct two-tone LDM driving. Using the same interferometric probes together with controlled quenches, we reveal phase-dependent modifications of the Floquet bands and infer how the gap windings add or cancel. Sec. IV summarizes the results and discusses future outlook.

II. EXPERIMENTAL RESULT

Our experiment realizes a one-dimensional, spin-independent optical lattice described by

$$\begin{aligned} H(t) &= H_0 + H_m(t), \\ H_0 &= \frac{\hat{p}^2}{2m} + \frac{1}{2}V_0 \cos(2k_L x), \\ H_m(t) &= \frac{1}{2}\delta V(t) \cos(2k_L x), \end{aligned} \quad (1)$$

where $k_L = 2\pi/\lambda$ with $\lambda \simeq 1064$ nm. Here $V_0 > 0$ and $\delta V(t)$ denote the static and time-dependent lattice depths, respectively. The recoil energy is $E_r = \hbar^2 k_L^2/(2m)$, with $E_r/h \simeq 2.02$ kHz. We choose the modulation to have zero time average over one period, i.e., $\langle \delta V(t) \rangle_T = 0$.

Restricting to the s and p orbitals, we write the driven lattice in a tight-binding form,

$$\hat{H}(t) = \sum_i \hat{\Psi}_i^\dagger M(t) \hat{\Psi}_i + \sum_i \left[\hat{\Psi}_i^\dagger J(t) \hat{\Psi}_{i+1} + \text{h.c.} \right], \quad (2)$$

where $\hat{\Psi}_i^\dagger = (\hat{a}_{i,p}^\dagger, \hat{a}_{i,s}^\dagger)$ and $\hat{a}_{i,\alpha}^\dagger$ creates an atom in orbital $\alpha = s, p$ on site i . The onsite matrix and nearest-neighbor coupling matrix are

$$M(t) = \begin{pmatrix} \epsilon_p & 0 \\ 0 & \epsilon_s \end{pmatrix} + \begin{pmatrix} \nu_0^{pp} & 0 \\ 0 & \nu_0^{ss} \end{pmatrix} \delta V(t) \quad (3)$$

and

$$J(t) = \begin{pmatrix} \tilde{t}_p & 0 \\ 0 & t_s \end{pmatrix} + \begin{pmatrix} \nu_1^{pp} & \nu_1^{ps} \\ -\nu_1^{ps} & \nu_1^{ss} \end{pmatrix} \delta V(t). \quad (4)$$

Here $\epsilon_{s/p}$ are the onsite energies for the static lattice H_0 . The coefficients $\nu_0^{\alpha\alpha} \equiv \frac{1}{2} \int dx w_\alpha^*(x-x_i) \cos(2k_L x) w_\alpha(x-x_i)$ describe the modulation-induced onsite shifts, and $\nu_1^{\alpha\beta} \equiv \frac{1}{2} \int dx w_\alpha^*(x-x_i) \cos(2k_L x) w_\beta(x-x_{i+1})$ with $\alpha\beta \in \{ss, pp, ps\}$ quantify the LDM-induced modification of the nearest-neighbor couplings. Because the p -orbital Wannier function has odd parity, the LDM-induced s - p coupling changes sign under bond reversal, which provides the antisymmetric coupling structure required for a nontrivial band topology (Fig. 1(a)(b)).

We transform to quasimomentum space via $\hat{\Psi}_k^\dagger = \frac{1}{\sqrt{N}} \sum_j e^{ikj} \hat{\Psi}_j^\dagger$, giving $\hat{H}(t) = \sum_k \hat{\Psi}_k^\dagger \hat{H}_k(t) \hat{\Psi}_k$. For a minimal description, we replace the p -band dispersion by $\tilde{t}_p \cos k$ and fix \tilde{t}_p by matching the bandwidth of a third-order cosine expansion [41]. This approximation preserves the relevant gap openings and therefore does not affect the topology. For single-tone driving $\delta V(t) = \delta V_0 \cos(\omega_0 t + \phi_0)$, the time-independent effective Floquet Hamiltonian near the gap-opening momenta takes the form [42]

$$H_F^{(j)}(k) = \sum_{i=y,z} h_{F,i}^{(j)}(k) \sigma_i + h_{F,0}^{(j)}(k) \sigma_0, \quad (5)$$

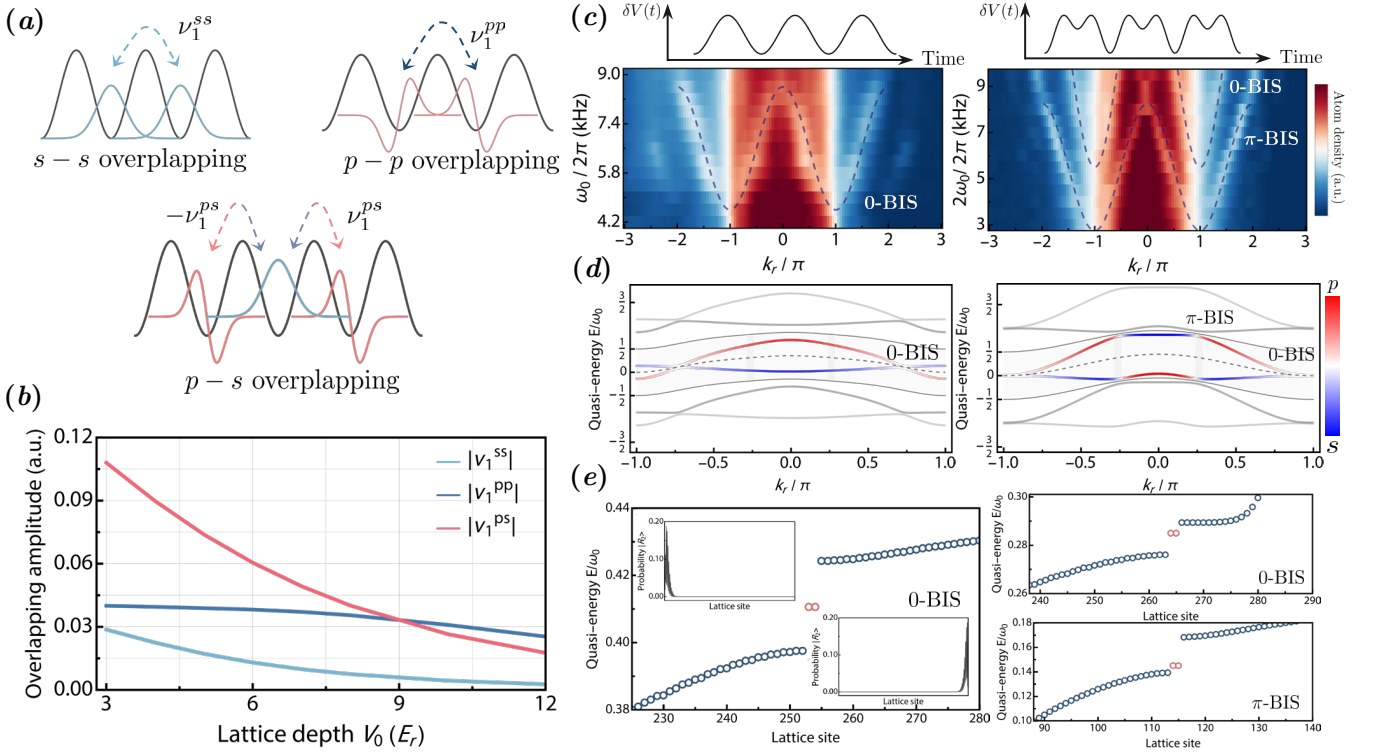


FIG. 1. Topology from lattice-depth modulation (LDM) and the corresponding Floquet band structures for single- and two-tone driving. (a) A gauge transformation $w_p(x) \rightarrow (-1)^j w_p(x)$ renders the p -orbital hopping spatially uniform while keeping the s - p coupling staggered. (b) Nearest-neighbor overlap coefficients $\nu_1^{\alpha\beta}$ for the s - s , p - p , and p - s channels. The adjacent s and p Wannier overlap remains sizable up to $V_0 = 10 E_r$. (c) Experimental measurements for single-tone driving at ω_0 with $\delta V_0 = 0.875 E_r$, and for two-tone driving at ω_0 and $2\omega_0$ with $\delta V_0^{(1)} = \delta V_0^{(2)} = 0.875 E_r$, both at lattice depth $V_0 = 3.5 E_r$. All data are extracted from time-of-flight (TOF) images taken after 30 ms of expansion. Each slice is averaged over five shots. (d,e) Numerical Floquet bands for single-tone driving with $\omega_0 = 5 E_r/\hbar$ and $\delta V_0 = 0.5 E_r$, and for two-tone driving at $\omega_0 = 4 E_r/\hbar$ and $2\omega_0$ with $\delta V_0^{(1)} = 0.5 E_r$ and $\delta V_0^{(2)} = 1 E_r$. Simulations use $V_0 = 4.5 E_r$ to enhance the visibility of the two pairs of edge states.

with ($j = 1$ for the single-tone channel)

$$\begin{aligned}
 h_{F,y}^{(1)}(k) &= -\delta V_0 \nu_1^{ps} \sin k, \\
 h_{F,z}^{(1)}(k) &= \frac{1}{2} [\epsilon_p - \epsilon_s - \omega_0 + 2(\tilde{t}_p - t_s) \cos k], \\
 h_{F,0}^{(1)}(k) &= \frac{1}{2} [\epsilon_p + \epsilon_s - \omega_0 + 2(\tilde{t}_p + t_s) \cos k]. \quad (6)
 \end{aligned}$$

Here σ_i are Pauli matrices, σ_0 is the identity matrix. The index j labels the resonant channel and equivalently labels the BIS pair (and associated gap) opened by that channel in our setup. The Floquet generator $H_F^{(j)}(k)$ reproduces the stroboscopic evolution at integer multiples of the drive period $T = 2\pi/\omega_0$.

Even when the modulation satisfies the even-time constraint $H_m(t+t_\phi) = H_m(t-t_\phi)$ for $0 \leq t_\phi = \phi_0/\omega_0 < T$, a nonzero $h_{F,0}(k)$ breaks the conventional chiral symmetry. The realized Floquet topological phase is nevertheless a symmetry-protected topological phase whose topology is guaranteed jointly by a magnetic group symmetry and a nonlocal chiral symmetry, which together forces the two edge states $|\phi_{L/R}\rangle$ lie at non-zero quasienergy [43]. For simplicity, unless stated otherwise we work in the

even-time driving convention and ignore explicit phase dependence in Eqs. 5 and 6. Therefore, the stroboscopic Floquet Hamiltonian coincide for our purposes.

According to standard Floquet theory, periodic driving generates a quasienergy band structure that can be tuned via the drive period T . A modulation at frequency ω_0 exchanges energy quanta $n\omega_0$ ($n \in \mathbb{Z}$) with the static system ($\delta V_0 = 0$). In the weak-modulation regime, the Floquet bands can be understood by copying the static bands of H_0 , shifting them by $n\omega_0$, and folding them into the quasienergy FBZ $E \in [-\omega_0/2, \omega_0/2]$, up to an additional k -dependent shift $h_{F,0}(k)$. Fig. 1(c) illustrates, for single- and two-harmonic driving in our experiment, situations where the folded band replicas cross once and twice within the FBZ. The coupling term $h_{F,y}(k)$ hybridizes the replicated bands and opens gaps at the crossings. In the two-crossing case, this can realize either high-winding or vanishing-winding Floquet topology. Typical dispersions are shown in Fig. 1(d,e).

The bulk topology of the driven system can be characterized by a zero-dimensional BIS invariant. For the j th BIS, defined by the momenta $k_{j,L/R}$ satisfying

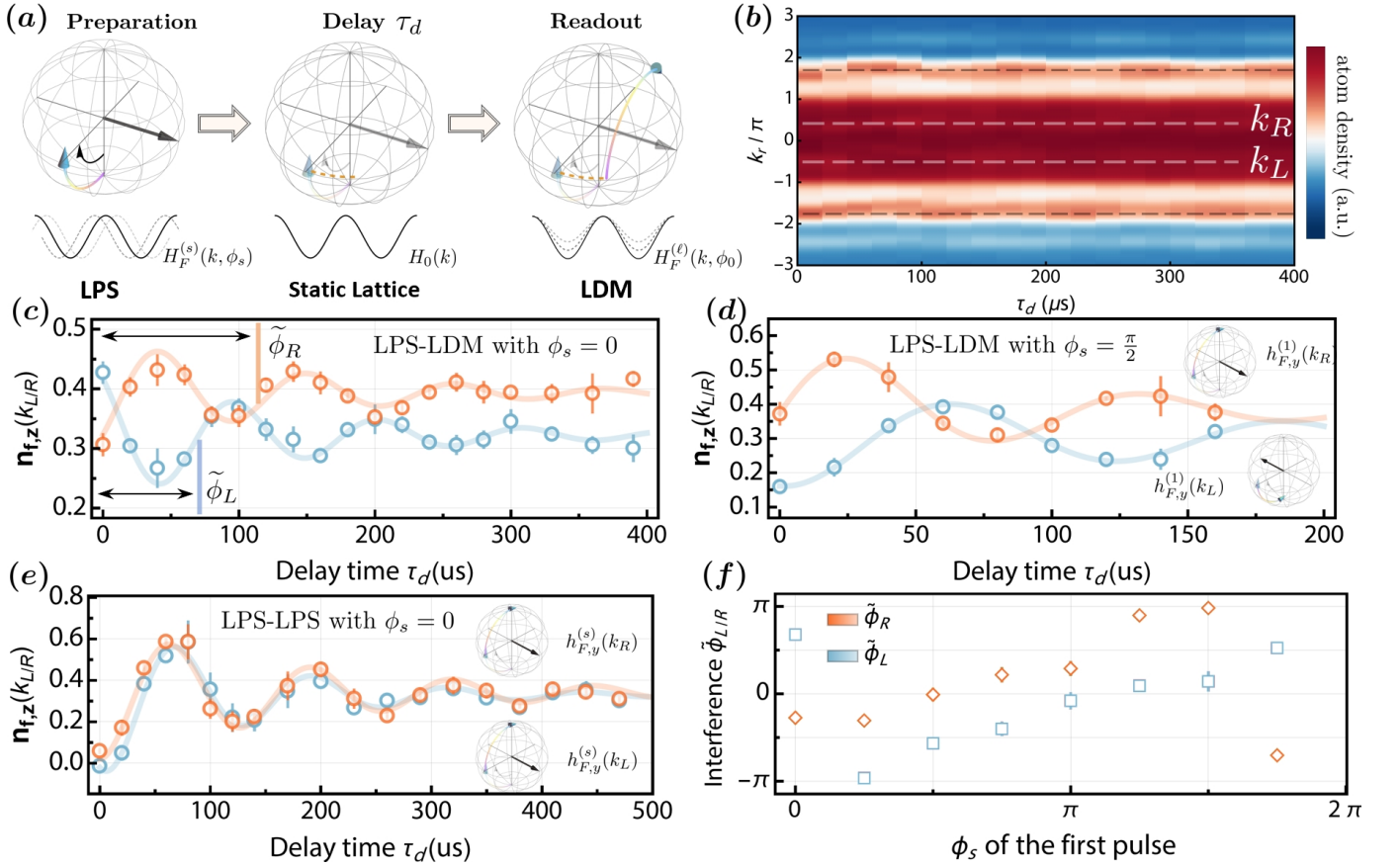


FIG. 2. Ramsey detection of the single-photon s - p resonance induced by single-tone lattice-depth modulation (LDM) at the BIS momenta. (a) The Ramsey sequence uses a lattice-position shaking (LPS) preparation pulse with stroboscopic form $H_F^{(s)}(k, \phi_s)$ and duration t_1 , followed by a dark evolution of duration τ_d under the static Hamiltonian H_0 , and a LDM readout described by $H_F^{(l)}(k, \phi_0 = 0)$ with duration t_2 . All pulses are set close to $\pi/2$ to maximize fringe contrast. (b) Atomic momentum space density during the sequence in experiment. (c-d) Ramsey fringes of the spin imbalance at the two BIS $k = k_R$ (yellow dots) and $k = k_L$ (blue dots) for the LPS-LDM sequence as τ_d is varied. The preparation phase choices are $\phi^{(s)} = 0$ and π . A robust π phase shift between k_R and k_L is observed. (e) LPS-LPS sequence showing no phase shift between the two BIS fringes. (f) In the LPS-LDM sequence, the LPS preparation phase ϕ_s sets the global fringe phase, while the relative π contrast between k_R and k_L is preserved. The fitting function is $\tilde{n}_{f,z}(k) = \sin(\frac{2\pi}{T}t + \tilde{\phi}) \exp(-\lambda t) + \tilde{c}$, where tildes denote fitted parameters. The experimental parameters are $\delta D = 22.3$ nm for the LPS with $t_1 = 2T$ and $\delta V_0 = 1.2 E_r$ for the LDM with $t_2 = 4T$. The drive period is $T = 2\pi/\omega_0$ with $\omega_0 = 2\pi \times 8$ kHz and $V_0 = 3.5 E_r$ for static lattice.

$h_{F,z}(k_{j,L/R}) = 0$, the corresponding invariant reads

$$\nu_j = \frac{1}{2} \left\{ \text{sgn}[h_{F,y}(k_{j,R})] - \text{sgn}[h_{F,y}(k_{j,L})] \right\}. \quad (7)$$

We divide BISs into π -BISs and 0-BISs, depending on whether they occur at the boundary or at the center of the FBZ. Then the total winding number of the Floquet bands is

$$W = \sum_j (-1)^{\alpha_j/\pi} \nu_j, \quad (8)$$

where $\alpha_j = 0$ or π for a 0-BIS or a π -BIS, respectively. Finally, the gap invariants $W_{0/\pi} = \sum_{\alpha_j=0/\pi} \nu_j$ determine the numbers of edge modes in the 0 and π gaps [32].

In our model, all BISs are drive induced because the static part H_0 provides no interband (s - p) coupling. Consequently, detection schemes that rely on a well-prepared

initial pseudospin polarization to extract time-averaged spin textures are not applicable. When the gaps are opened entirely by the drive, Ramsey interferometry provides a direct route to access the band phase at selected quasimomenta. Experimentally, we use a first-order LPS pulse as a topologically trivial preparation (beam-splitting) pulse to split the population initially prepared in the s band, as first demonstrated in Ref. [33]. After a controlled evolution time, we apply LDM as the interferometric readout pulse. In the weak-drive regime, choosing the two Ramsey pulses to have the same modulation frequency ensures that the interference probes essentially the same BIS.

The Ramsey interferometric measurement proceeds as shown in Fig. 2(a) using a mixed-modulation sequence: (i) we adiabatically load ^{87}Rb into the s band, prepar-

ing an initial population that nearly fills the band, at a temperature of about 105 nK; (ii) we abruptly couple the s and p bands using LPS for a duration t_1 , serving as a topologically trivial polarization pulse; (iii) the atoms are allowed to evolve in the static lattice for a time τ_d ; (iv) finally, we apply LDM as an interferometric projection pulse for a duration t_2 . The LPS takes the form $H_s = \hat{p}^2/2m + V_0 \cos[2k_L(x + x_s(t))]/2$, where $x_s(t) = \delta D \cos(\omega_s t + \phi_s)$ and δD is the maximum displacement. This periodic drive defines the stroboscopic Floquet Hamiltonian $H_F^{(s)}(k, \phi_s) = \sum_i h_{F,i}^{(s)}(k, \phi_s) \sigma_i + h_{F,0}^{(s)}(k) \sigma_0$, where the superscript s denotes the LPS Floquet Hamiltonian. We define the spin imbalance $\langle \sigma_z(k) \rangle = [n_s(k) - n_p(k)]/[n_s(k) + n_p(k)] \equiv n_{f,z}(k)$ as the Ramsey interferometric signal, where $n_{s(p)}(k)$ denotes the momentum-space density in the s (p) orbital.

The spin imbalance after the interferometric process reads [42]

$$n_{f,z}(k) = -[\mathcal{A}(k) + \mathcal{V}(k) \cos[\Phi(k) - \Phi_0(k)]]. \quad (9)$$

Since the topological invariants are read from the BIS, we focus on momenta where $h_{F,z}^{(j)}(k_{j,L/R}) = 0$ and choose the two pulses to be near $\pi/2$ pulses by setting t_1 and t_2 to proper integer multiples of the period, which suppresses micromotion and ensures the validity of the stroboscopic Hamiltonian. The phase accumulated during the interval τ_d is $\Phi_0(k) = \Delta\phi = \phi_s - \arg[\mathbf{h}_F^{(j)}(k_{j,L/R})] + \omega_s t_1 + (\epsilon_p - \epsilon_s)\tau_d$, and $\Phi(k) = 2h_{F,z}^{(s)}(k_{j,L/R})\tau_d \approx 0$ in the weak-drive regime. In Fig. 2(b), we show the Ramsey fringe evolution for single-harmonic driving, where only one BIS pair appears at k_L and k_R . The Ramsey evolution of $n_{f,z}$ in Fig. 2(c) clearly exhibits an approximately π phase difference between these two points, consistent with $h_{F,y}^{(1)}(k_L) = -h_{F,y}^{(1)}(k_R)$.

From the fits, we obtain oscillation periods $\tilde{T} = 107(2) \mu\text{s}$ at $k_{1,L}$ and $109(3) \mu\text{s}$ at $k_{1,R}$. By contrast, if the two Ramsey pulses both consist of LPS, the coupling is trivial since $h_{F,y}^{(s)}(k_{1,L}) = h_{F,y}^{(s)}(k_{1,R})$, and the spin-imbalance evolution is in phase, $\phi_L(\tau) = \phi_R(\tau)$, as shown in Fig. 2(e). The period of the Ramsey fringes is $\tilde{T} = 126(2) \mu\text{s}$, which is closer to the shaking period $2\pi/\omega_0$.

In practice, the momentum signals produced by the LPS and LDM pulses largely overlap, so we analyze the response near the peak where the two cloud centers cannot be reliably distinguished. Empirically, the LPS-LDM sequence yields faster fringes, whereas the LPS-LPS sequence shows slower fringes with a period close to the shaking period ($\tilde{T} \approx 2\pi/\omega_0$). This behavior is consistent with a small pulse-dependent shift of the stroboscopic BIS arising from different higher-order Floquet corrections for the two pulse types, which produces a finite detuning at the selected quasimomentum. When we tune the initial phase ϕ_s from 0 to 2π , the fitted initial phases $\tilde{\phi}_{R(L)}$ shift accordingly, while the relative π phase difference between the two BIS momenta of a given pair, k_L

and k_R , remains robust, as shown in Fig. 2(f).

III. TWO-TONE COHERENT MODULATION

We next consider a two-tone LDM that simultaneously addresses the ω_0 and $2\omega_0$ resonances through the first-order resonant couplings. The modulation is taken as

$$\delta V(t) = \delta V_0^{(1)} \cos(\omega_0 t + \phi_0^{(1)}) + \delta V_0^{(2)} \cos(2\omega_0 t + \phi_0^{(2)}), \quad (10)$$

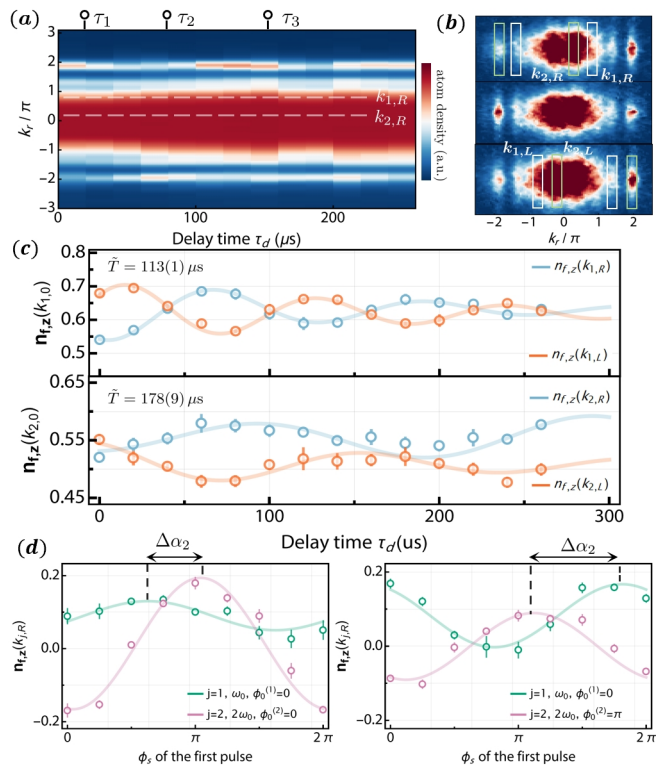


FIG. 3. Ramsey interferometry with two-tone driving ($\omega_0, 2\omega_0$). (a-b) State preparation uses a two-tone LPS pulse, which launches coherent evolution governed by the Bloch equation of motion. Readout uses a two-tone LDM pulse with matching frequency components so that both BIS pairs ($k_{j,L}, k_{j,R}$) for $j = 1, 2$ are addressed. Here $\tau_{1,2,3}$ label data taken at $\tau_d = 20 \mu\text{s}$, $80 \mu\text{s}$, and $160 \mu\text{s}$, respectively. (c) A characteristic π phase contrast between the left and right BIS momenta in either the 0 gap or the π gap indicates opposite orientations of the effective Bloch field, consistent with $h_{F,y}(-k) = -h_{F,y}(k)$ on the BIS. (d) Zero-delay Ramsey readout for two settings of the interferometric pulse phase, $\phi_0^{(2)} = 0$ and π . Toggling $\phi_0^{(2)}$ produces a global π shift of the interferometric phase and reverses the relative phase between the $j = 1$ and $j = 2$ BIS pairs. The experimental parameters are $\delta V_0^{(1)} = \delta V_0^{(2)} = 0.98 E_r$ for LDM. For the preparation LPS pulse, $\delta D^{(1)} = \delta D^{(2)} = 22.3 \text{ nm}$ and $\phi_s^{(1)} = \phi_s^{(2)} = \phi_s$, with a duration of $250 \mu\text{s}$. The modulation frequencies are ω_0 and $2\omega_0$, where $\omega_0 = 2\pi \times 4 \text{ kHz}$. The static lattice depth is $V_0 = 3.5 E_r$.

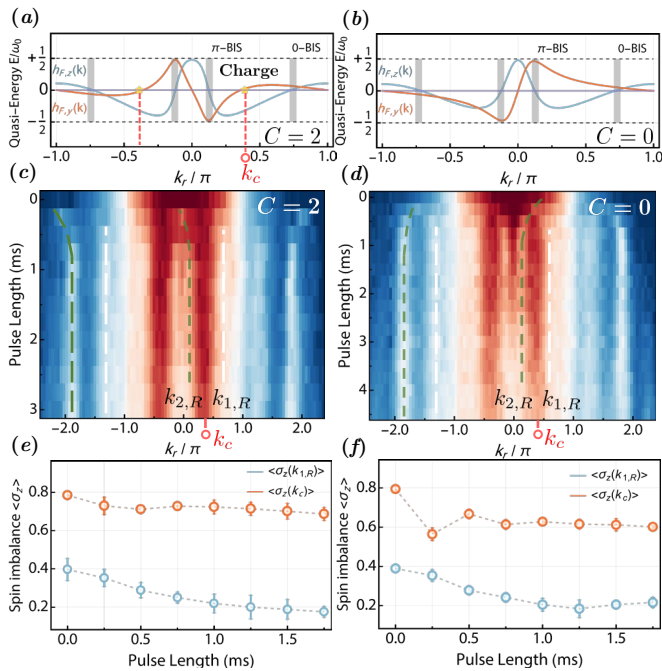


FIG. 4. Measurement of the dynamics at the topological charge momentum k_c , defined by $h_{F,y}(k_c) = 0$. (a) For $\phi_0^{(2)} = 0$, the total winding number of the Floquet bands is $C = 2$. A topological charge occurs at $k_c \approx 0.4\pi$, which suppresses the transverse drive and results in nearly frozen dynamics in (e). (b) For $\phi_0^{(2)} = \pi$, the total winding number is $C = 0$. No charge lies between the BIS momenta, so $|h_{F,y}(k_c)|$ remains finite and damped s - p oscillations are observed in (d). Dashed lines are guides to the eye. The color scale and the experimental LDM-pulse parameters are the same as in Fig. 3. The calculated effective Floquet Hamiltonian components $h_{F,y}(k)$ and $h_{F,z}(k)$ are obtained using the same parameters.

with the phase reference chosen as $\phi_0^{(1)} = 0$ and $\phi_0^{(2)} = 0$ or π to preserve the even-time driving convention used throughout. The relative phase of the second harmonic, $\phi_0^{(2)}$, not only modifies the Floquet couplings but can qualitatively change the topology of the driven bands and the resulting observables away from simple resonance conditions. In earlier two-tone LPS schemes, by contrast, the relative phase is used to break time-reversal symmetry and thereby selectively close a gap at one of the two BIS momenta (e.g., at k_R but not at k_L), rather than to create additional BIS pairs and control multiple gaps in a gap-resolved manner [34, 35, 44]. Moreover, for realizing an anomalous Floquet phase in an orbital-ladder scheme, frequency-doubled two-tone LPS is not clean, since the $2\omega_0$ component generically introduces a first-order trivial channel that masks the intended two-photon topological coupling generated by the ω_0 drive.

The two-tone drive in our scheme produces two drive-induced BIS pairs: the 0-BIS pair ($j = 1$) and the π -BIS pair ($j = 2$). The 0-BIS is described by the Floquet Hamiltonian $H_F^{(j=1)}(k)$ in Eqs. 5 and 6. The π -BIS is

governed by a second Floquet Hamiltonian with the same Pauli-matrix decomposition as Eq. 5, but with different components. The leading terms (including the dominant two-photon contribution induced by the $j = 1$ channel) are

$$\begin{aligned} h_{F,y}^{(2)}(k) &\simeq -\left[\delta V_0^{(2)} e^{-i\phi_0^{(2)}} + \delta V_0^{(1)} J_1\left(\frac{\delta V_0^{(1)}}{\omega_0}\right)\right] v_1^{ps} \sin k, \\ h_{F,z}^{(2)}(k) &= \frac{1}{2}[\epsilon_p - \epsilon_s - 2\omega_0 + 2(\tilde{t}_p - t_s) \cos k], \\ h_{F,0}^{(2)}(k) &= \frac{1}{2}[\epsilon_p + \epsilon_s - 2\omega_0 + 2(\tilde{t}_p + t_s) \cos k], \end{aligned} \quad (11)$$

where $J_n(z)$ is the Bessel function of the first kind. In the regime realized in our experiment the direct second-harmonic term dominates, i.e. $\delta V_0^{(2)} \gg \delta V_0^{(1)} J_1(\delta V_0^{(1)}/\omega_0)$, so the gap at the momenta $k_{2,L/R}$ defined by $h_{F,z}^{(2)}(k_{2,L/R}) = 0$ is set primarily by the amplitude and phase of the second-harmonic drive. Crucially, for $\phi_0^{(2)} = 0$ or π the relative sign of $h_{F,y}^{(2)}$ with respect to $h_{F,y}^{(1)}$ (in the same frame) is controlled by $\phi_0^{(2)}$, so the two BIS pairs can contribute additively or subtractively to the net winding of the Floquet bands. This phase control enables access to distinct configurations of (W_0, W_π) .

For experimental detection, we employ the same Ramsey protocol described above. A two-tone LPS pulse with frequency components $\omega_s = \omega_0$ and $2\omega_0$, whose stroboscopic Floquet Hamiltonian is denoted by $H_F^{(s,j)}$, prepares Bloch states at the BIS momenta $k_{j,L/R}$ for $j = 1, 2$. The second pulse is the two-tone LDM introduced before. By recording Ramsey fringes at the left and right momenta for each BIS pair j , we directly probe the relative phase of the transverse coupling field $h_{F,y}^{(j)}(k_{j,L/R})$. The results, shown in Fig. 3, demonstrate that the Ramsey fringes retain an approximately π phase difference between $k_{j,L}$ and $k_{j,R}$ for each BIS pair. The measured Ramsey periods are $\tilde{T} = 178(9) \mu\text{s}$ for the π -BIS and $\tilde{T} = 113(1) \mu\text{s}$ for the 0-BIS. As a consequence of this period shift, the topology cannot be inferred solely from the initial Ramsey phase using the simple form of Eq. 9.

We next examine the role of the second-tone phase $\phi_0^{(2)}$ using two consecutive pulses with zero inter-pulse delay ($\tau_d = 0$). The preparation is a two-tone LPS pulse with initial phases $\phi_s^{(j=1)} = \phi_s^{(j=2)} \equiv \phi_s$ and pulse area close to $\pi/2$, which places the Bloch vector near the equator at the BISs. The readout is a two-tone LDM pulse that is far shorter than a $\pi/2$ pulse and therefore acts in the linear-response regime, mainly imprinting the axis phase of the second tone. In this limit the phase contrast between the signals $n_{f,z}$ at the 0-BIS ($j = 1$) and the π -BIS ($j = 2$) is set by $\Delta\alpha_2 = \arg[h_{F,y}^{(2)}(k_{2,L/R})] - \arg[h_{F,y}^{(1)}(k_{1,L/R})]$. Fig. 4(d) compares $\phi_0^{(2)} = 0$ and $\phi_0^{(2)} = \pi$ with $\phi_0^{(1)} = 0$ fixed. Fits give $\Delta\alpha_2 = 74^\circ$ and -124° , which differ by nearly π and indicate that toggling $\phi_0^{(2)}$ reverses the orientation of the effective Bloch field $\mathbf{h}_F^{(2)}(k_{2,L/R})$ relative to $\mathbf{h}_F^{(1)}(k_{1,L/R})$.

Moreover, the two-tone LDM can qualitatively reshape

the Floquet band structure away from the BIS momenta in a way controlled by the relative phase $\phi_0^{(2)}$. We compute the Floquet bands in the first Brillouin zone for $\phi_0^{(2)} = 0$ and π , using a common gauge for the 0- and π -gap sectors [Fig. 4(a,b)]. For $\phi_0^{(2)} = 0$ we find $(W_0, W_\pi) = (1, 1)$, giving a total winding $W = 2$, while for $\phi_0^{(2)} = \pi$ we obtain $(W_0, W_\pi) = (1, -1)$, yielding $W = 0$ [42]. In both cases, the topology is specified gap by gap through (W_0, W_π) , and the nonzero π -gap winding highlights an intrinsically Floquet phase with no static analogue. Notably, at $\phi_0^{(2)} = \pi$ the net winding cancels, while the topological edge modes remain in the 0 and π gaps.

When $\phi_0^{(2)} = 0$, $h_{F,y}(k)$ crosses zero between the two BIS at a momentum $k = k_c$, reversing the sign of the effective transverse coupling. This defines a topological charge of the effective Bloch field, where $h_{F,y}(k_c) = 0$ while $h_{F,z}(k_c) \neq 0$ [45]. We reveal this feature by measuring the spin imbalance $\langle \sigma_z \rangle$ after a two-tone LDM pulse. Fig. 4(c,f) compare the two phase choices. For $\phi_0^{(2)} = 0$, a node appears near $k_c \approx 0.4\pi$ and the dynamics at that point are strongly suppressed, consistent with a vanishing coupling, i.e., $h_{F,y}(k_c) = 0$. For $\phi_0^{(2)} = \pi$, there is no node between the BISs and the dynamics near the midpoint show fast, damped s - p oscillations. The response near $k_{1,R}$ remains nearly the same in both cases. Although the coherent two-tone LDM modifies the overall coupling strength, it does not produce a pronounced change in the measured dynamics at $k_{1,R}$ for our parameters, indicating that the observed contrast at k_c is consistent with the emergence of the $h_{F,y} = 0$ node for $\phi_0^{(2)} = 0$.

IV. CONCLUDING REMARKS

In conclusion, we have realized a controllable, gap-resolved Floquet topological phase in a one-dimensional optical lattice. Beyond demonstrating multi-frequency control, we identify and exploit a commonly neglected ingredient of lattice depth modulation, namely the sizable nearest-neighbor s - p overlap in a lattice. Owing

to the odd parity of the p orbital, this overlap generates a staggered s - p coupling with the sign structure required for minimal nontrivial Floquet topology. Building on this mechanism, a two-tone drive with a tunable relative phase sets the effective coupling signs in the 0 and π gaps individually. We read out the gap windings (W_0, W_π) with a BIS-resolved Ramsey protocol. Controlled quenches further reveal distinct dynamics at quasimomenta far from resonance, demonstrating that tuning the relative phase between the two tones not only reshapes the BIS structure but also induces a global change in the topology of the Floquet bands.

These results have three implications. First, lattice depth modulation remains topologically robust once realistic nearest-neighbor s - p overlaps are included, establishing LDM as a quantitatively reliable knob for engineering orbital couplings and synthetic gauge flux in optical lattices [46–48]. Second, coherent multi-tone driving provides phase-tunable control of the sign pattern of the gap windings, while the BIS-resolved Ramsey protocol offers a compact, interferometric readout of the gap windings, performed gap-by-gap. Third, lattice position shaking and depth modulation, including multiple harmonics, can be combined phase coherently within a single sequence, enabling mixed-drive protocols with independently addressable gaps. Together, these capabilities make multi-frequency phase control a quantitative tool for preparing and benchmarking a wide range of (W_0, W_π) configurations, and establish phase-coherent mixed modulation as a practical route to mixed-drive schemes targeting high-winding Floquet phases [49–51].

Acknowledgements. We thank Long Zhang for fruitful discussions and for reading the manuscript. We also thank Zijie Zhu for helpful comments. This work was supported by National Key Research and Development Program of China (2021YFA1400900), the National Natural Science Foundation of China (Grants No. 12425401 and No. 12261160368), and the Quantum Science and Technology-National Science and Technology Major Project (Grant No. 2021ZD0302000).

Author contributions. P.J.Z. and Y.D.W. contributed equally to this work.

-
- [1] A. Eckardt, *Reviews of Modern Physics* **89**, 011004 (2017).
 - [2] M. S. Rudner and N. H. Lindner, *Nature Reviews Physics* **2**, 229 (2020).
 - [3] C. Weitenberg and J. Simonet, *Nature Physics* **17**, 1342 (2021).
 - [4] T. Oka and H. Aoki, *Phys. Rev. B* **79**, 081406 (2009).
 - [5] T. Kitagawa, E. Berg, M. Rudner, and E. Demler, *Phys. Rev. B* **82**, 235114 (2010).
 - [6] M. C. Rechtsman, J. M. Zeuner, Y. Plotnik, Y. Lumer, D. Podolsky, F. Dreisow, S. Nolte, M. Segev, and A. Szameit, *Nature* **496**, 196 (2013).
 - [7] N. Goldman and J. Dalibard, *Phys. Rev. X* **4**, 031027 (2014).
 - [8] G. Jotzu, M. Messer, R. Desbuquois, M. Lebrat, T. Uehlinger, D. Greif, and T. Esslinger, *Nature* **515**, 237 (2014).
 - [9] W. Zheng and H. Zhai, *Physical Review A* **89**, 061603 (2014).
 - [10] M. Bukov, L. D’Alessio, and A. Polkovnikov, *Advances in Physics* **64**, 139 (2015).
 - [11] A. Eckardt and E. Anisimovas, *New Journal of Physics* **17**, 093039 (2015).
 - [12] N. Fläschner, B. S. Rem, M. Tarnowski, D. Vogel, D.-

- S. Lühmann, K. Sengstock, and C. Weitenberg, *Science* **352**, 1091 (2016).
- [13] M. S. Rudner, N. H. Lindner, E. Berg, and M. Levin, *Phys. Rev. X* **3**, 031005 (2013).
- [14] J. K. Asbóth, B. Tarasinski, and P. Delplace, *Phys. Rev. B* **90**, 125143 (2014).
- [15] F. Nathan and M. S. Rudner, *New Journal of Physics* **17**, 125014 (2015).
- [16] D. Carpentier, P. Delplace, M. Fruchart, and K. Gawędzki, *Phys. Rev. Lett.* **114**, 106806 (2015).
- [17] L. Zhang and X.-J. Liu, *PRX Quantum* **3**, 040312 (2022).
- [18] D. Leykam, M. C. Rechtsman, and Y. D. Chong, *Phys. Rev. Lett.* **117**, 013902 (2016).
- [19] F. Nathan, D. Abanin, E. Berg, N. H. Lindner, and M. S. Rudner, *Phys. Rev. B* **99**, 195133 (2019).
- [20] L. J. Maczewsky, J. M. Zeuner, S. Nolte, and A. Szameit, *Nature communications* **8**, 13756 (2017).
- [21] S. Mukherjee, A. Spracklen, M. Valiente, E. Andersson, P. Öhberg, N. Goldman, and R. R. Thomson, *Nature communications* **8**, 13918 (2017).
- [22] C. Chen, X. Ding, J. Qin, J. Wu, Y. He, C.-Y. Lu, L. Li, X.-J. Liu, B. C. Sanders, and J.-W. Pan, *Phys. Rev. Lett.* **129**, 046401 (2022).
- [23] Z. Zhang, J. Wang, H. Qin, and R. Fleury, *Optical Materials Express* **15**, 828 (2025).
- [24] Q. Cheng, Y. Pan, H. Wang, C. Zhang, D. Yu, A. Gover, H. Zhang, T. Li, L. Zhou, and S. Zhu, *Phys. Rev. Lett.* **122**, 173901 (2019).
- [25] M. Li, C. Li, L. Yan, Q. Li, Q. Gong, and Y. Li, *Light: Science & Applications* **12**, 262 (2023).
- [26] N. R. Cooper, J. Dalibard, and I. B. Spielman, *Reviews of Modern Physics* **91**, 015005 (2019).
- [27] I. Bouchoule, R. Citro, T. Duty, T. Giamarchi, R. G. Hulet, M. Klanjšek, E. Orignac, and B. Weber, *Nature Reviews Physics* **7**, 565 (2025).
- [28] D. Xie, T.-S. Deng, T. Xiao, W. Gou, T. Chen, W. Yi, and B. Yan, *Phys. Rev. Lett.* **124**, 050502 (2020).
- [29] K. Wintersperger, C. Braun, F. N. Únal, A. Eckardt, M. D. Liberto, N. Goldman, I. Bloch, and M. Aidelsburger, *Nature Physics* **16**, 1058 (2020).
- [30] M. Lu, G. H. Reid, A. R. Fritsch, A. M. Piñeiro, and I. B. Spielman, *Phys. Rev. Lett.* **129**, 040402 (2022).
- [31] J.-Y. Zhang, C.-R. Yi, L. Zhang, R.-H. Jiao, K.-Y. Shi, H. Yuan, W. Zhang, X.-J. Liu, S. Chen, and J.-W. Pan, *Physical Review Letters* **130**, 043201 (2023).
- [32] L. Zhang, L. Zhang, and X.-J. Liu, *Physical Review Letters* **125**, 183001 (2020).
- [33] J. H. Kang, J. H. Han, and Y. Shin, *New Journal of Physics* **22**, 013023 (2020).
- [34] J. Minguzzi, Z. Zhu, K. Sandholzer, A.-S. Walter, K. Viebahn, and T. Esslinger, *Phys. Rev. Lett.* **129**, 053201 (2022).
- [35] K. Sandholzer, A.-S. Walter, J. Minguzzi, Z. Zhu, K. Viebahn, and T. Esslinger, *Physical Review Research* **4**, 013056 (2022).
- [36] Y. Kiefer, M. Hachmann, and A. Hemmerich, *Nature Physics* **19**, 794 (2023).
- [37] V. Venu, P. Xu, M. Mamaev, F. Corapi, T. Bilitewski, J. P. D’Incao, C. J. Fujiwara, A. M. Rey, and J. H. Thywissen, *Nature* **613**, 262 (2023).
- [38] M. Creutz, *Phys. Rev. Lett.* **83**, 2636 (1999).
- [39] N. Sun and L.-K. Lim, *Phys. Rev. B* **96**, 035139 (2017).
- [40] J. Jünemann, A. Piga, S.-J. Ran, M. Lewenstein, M. Rizzi, and A. Bermudez, *Phys. Rev. X* **7**, 031057 (2017).
- [41] For a finite lattice depth, the p -band dispersion can be written more accurately as $\varepsilon_p(k) = \sum_{n \geq 1} t_p^{(n)} \cos(nk)$. For $V_0 = 3.5 E_r$ we obtain $t_p^{(1)} = 0.96 E_r$, $t_p^{(2)} = 0.14 E_r$, and $t_p^{(3)} = 0.077 E_r$. For a single-cosine surrogate $\varepsilon_p(k) \approx t_p \cos k$, we match the bandwidth and set $\tilde{t}_p = \sum_{\text{odd } n} t_p^{(n)} \approx 1.04 E_r$.
- [42] See Supplementary Materials for additional details.
- [43] B. Song, L. Zhang, C. He, T. F. J. Poon, E. Hajiyev, S. Zhang, X.-J. Liu, and G.-B. Jo, *Science Advances* **4**, eaao4748 (2018).
- [44] J. H. Kang and Y.-i. Shin, *Phys. Rev. A* **102**, 063315 (2020).
- [45] L. Zhang, L. Zhang, and X.-J. Liu, *Physical Review A* **100**, 063624 (2019).
- [46] X. Li, E. Zhao, and W. Vincent Liu, *Nature Communications* **4**, 1523 (2013).
- [47] J. Jünemann, A. Piga, S.-J. Ran, M. Lewenstein, M. Rizzi, and A. Bermudez, *Phys. Rev. X* **7**, 031057 (2017).
- [48] G. Rajeevan and S. Mukherjee, (2026), [arXiv:2601.08914](https://arxiv.org/abs/2601.08914).
- [49] H. Liu, T.-S. Xiong, W. Zhang, and J.-H. An, *Physical Review A* **100**, 023622 (2019).
- [50] K. Shi, X. Zhang, and W. Zhang, *Physical Review A* **109**, 013324 (2024).
- [51] D. Bae, J. Park, M. Kim, H. Kwak, J. Kwon, and Y. Shin, *Phys. Rev. Res.* **6**, 043122 (2024).

Supplementary Materials

I. EFFECTIVE HAMILTONIAN FOR MULTI-FREQUENCY LATTICE DEPTH MODULATION

In this section we derive a general effective Hamiltonian for a one-dimensional lattice with multi-harmonic depth modulation (LDM). We start from the continuum Hamiltonian

$$H(t) = \frac{\hat{p}^2}{2m} + \frac{1}{2}V_0 \cos(2k_L x) + \frac{1}{2}V_m(t) \cos(2k_L x). \quad (\text{S1})$$

We assume the modulation has the form $V_m(t) = \sum_{j \geq 1} \delta V^{(j)} \cos(j\omega t + \phi_j)$ with j being a positive integer. To preserve the even-time driving convention we set $\phi_j = 0$ or π . Expanding the Hamiltonian in the (s, p) -orbital basis gives the multi-frequency two-band lattice model used in the main text,

$$\hat{H}(t) = \sum_i \hat{\Psi}_i^\dagger M(t) \hat{\Psi}_i + \sum_i \left[\hat{\Psi}_i^\dagger J(t) \hat{\Psi}_{i+1} + \text{h.c.} \right], \quad (\text{S2})$$

with

$$M(t) = \begin{pmatrix} \epsilon_p & 0 \\ 0 & \epsilon_s \end{pmatrix} + \begin{pmatrix} v_0^{pp} & 0 \\ 0 & v_0^{ss} \end{pmatrix} V_m(t) \quad (\text{S3})$$

and

$$J(t) = \begin{pmatrix} t_p & 0 \\ 0 & t_s \end{pmatrix} + \begin{pmatrix} v_1^{pp} & v_1^{ps} \\ -v_1^{ps} & v_1^{ss} \end{pmatrix} V_m(t) \quad (\text{S4})$$

In momentum space the Hamiltonian becomes

$$\begin{aligned} \hat{H}(k, t) &= \begin{pmatrix} \epsilon_p + 2t_p \cos k & 0 \\ 0 & \epsilon_s + 2t_s \cos k \end{pmatrix} + V_m(t) \begin{pmatrix} v_0^{pp} + 2v_1^{pp} \cos k & 2iv_1^{ps} \sin k \\ -2iv_1^{ps} \sin k & v_0^{ss} + 2v_1^{ss} \cos k \end{pmatrix} \\ &= \Delta_z(k) \sigma_z + \Delta_0(k) \sigma_0 + V_m(t) [d_z(k) \sigma_z + d_0(k) \sigma_0 + d_y(k) \sigma_y], \end{aligned} \quad (\text{S5})$$

where we have defined

$$\begin{aligned} \Delta_z(k) &= \frac{\epsilon_p - \epsilon_s + 2(t_p - t_s) \cos k}{2}, \\ \Delta_0(k) &= \frac{\epsilon_p + \epsilon_s + 2(t_p + t_s) \cos k}{2}, \\ d_z(k) &= \frac{v_0^{pp} - v_0^{ss} + 2(v_1^{pp} - v_1^{ss}) \cos k}{2}, \\ d_y(k) &= -2v_1^{ps} \sin k, \\ d_0(k) &= \frac{v_0^{pp} + v_0^{ss} + 2(v_1^{pp} + v_1^{ss}) \cos k}{2}. \end{aligned} \quad (\text{S6})$$

We apply the time-dependent local unitary transformation

$$\begin{aligned} U &= \exp[-i\phi(t)\sigma_z/2], \\ \phi(t) &= 2\Delta_c t + 2d_z(k) \sum_{j \geq 1} \xi^{(j)} \sin(j\omega t + \phi_j), \end{aligned} \quad (\text{S7})$$

with $\xi^{(j)} \equiv \delta V^{(j)}/(j\omega)$. The rotated Hamiltonian $H_{\text{rot}} = U\hat{H}(k, t)U^\dagger - iU^\dagger \partial_t U$ becomes

$$\begin{aligned} H_{\text{rot}} &= [\Delta_z(k) - \Delta_c] \sigma_z + [\Delta_0(k) + d_0(k)V_m(t)] \sigma_0 + d_y(k)V_m(t) [\cos \phi(t) \sigma_y + \sin \phi(t) \sigma_x] \\ &= [\Delta_z(k) - \Delta_c] \sigma_z + [\Delta_0(k) + d_0(k)V_m(t)] \sigma_0 + [-ig(k, t) \sigma_+ + ig^*(k, t) \sigma_-], \end{aligned} \quad (\text{S8})$$

where $\Delta_c \equiv j\omega/2$ (for $j = \pm 1, \pm 2, \dots$) selects the resonant energy sector and we defined $\sigma_{\pm} = (\sigma_x \pm i\sigma_y)/2$.

All resonant couplings appear in the off-diagonal function

$$g(k, t) \equiv d_y(k)V_m(t)e^{i\phi(t)} = \sum_m g_{m-j}(k)e^{im\omega t}. \quad (\text{S9})$$

The Fourier coefficients $g_n(k)$ can be obtained using the Jacobi-Anger expansion after introducing $\beta^{(j)} \equiv 2d_z(k)\xi^{(j)}$,

$$e^{i\sum_{j \geq 1} \beta^{(j)}(k) \sin(j\omega t + \phi_j)} = \sum_{n \in \mathbb{Z}} c_n(k)e^{in\omega t}, \quad (\text{S10})$$

with

$$c_n(k) = \sum_{\{n_j\}: \sum j n_j = n} \prod_{j \geq 1} J_{n_j}(\beta^{(j)}) e^{in_j \phi_j}, \quad (\text{S11})$$

where $J_n(z)$ is the Bessel function of the first kind. One finds

$$g_n(k) = \frac{d_y(k)}{2} \sum_{j \geq 1} \delta V^{(j)} [e^{i\phi_j} c_{n-j}(k) + e^{-i\phi_j} c_{n+j}(k)]. \quad (\text{S12})$$

Expanding H_{rot} in Fourier components gives

$$\begin{aligned} H_{\text{rot}} = & [\Delta_z(k) - \frac{j\omega}{2}] \sigma_z + [\Delta_0(k) + d_0(k)V_m(t)] \sigma_0 \\ & + \sum_m \left[-i g_{m-j}(k) e^{im\omega t} \sigma_+ + i g_{m-j}^*(k) e^{-im\omega t} \sigma_- \right]. \end{aligned} \quad (\text{S13})$$

Under the even-time driving convention ($\phi_j = 0$ or π) the coefficients $c_n(k)$ and $g_n(k)$ are real, so the Hamiltonian in Eq. (S13) does not contain a σ_x term (ignoring σ_0), which is consistent with the conventional chiral-symmetry structure of the model. Moreover, the time average of the scalar part vanishes:

$$\langle d_0(k)V_m \rangle_T = \frac{1}{T} \int_0^T d_0(k)V_m(\tau) d\tau = 0 \quad (\text{S14})$$

for even-time driving.

Resonant (time-independent) off-diagonal terms correspond to $m = 0$, i.e. $g_{m-j}(k) = g_{-j}(k)$. Retaining only these resonant components yields the effective Floquet Hamiltonian for the j -th channel,

$$H_F^{(j)} = \left[\Delta_z(k) - \frac{j\omega}{2} \right] \sigma_z + \Delta_0(k) \sigma_0 + \left[-i g_{-j}(k) \sigma_+ + i g_{-j}^*(k) \sigma_- \right]. \quad (\text{S15})$$

Off-resonant harmonics give rise to Bloch-Siegert type shifts of the resonant sector. These shifts can be computed perturbatively by summing the contributions from $m \neq j$. Since it is relatively small compared to the modulation frequency and it does not change the topology, we drop this term in our model.

II. APPLICATIONS: SINGLE- AND TWO-TONE DRIVING

For single-harmonic driving ($j = 1$) with $\phi_1 = 0$ for LDM, Eq. (S12) gives

$$\begin{aligned} g_{-j}(k) &= \frac{d_y(k)}{2} \delta V^{(1)} [e^{i\phi_1} c_{-j-1}(k) + e^{-i\phi_1} c_{-j+1}(k)] \\ &= \frac{d_y(k)}{2} \delta V^{(1)} [J_{-j-1}(\beta^{(1)}) + J_{-j+1}(\beta^{(1)})] \\ &= \frac{d_y(k)}{2} \delta V^{(1)} \frac{(-1)^{j+1} 2j J_j(\beta^{(1)})}{\beta^{(1)}}. \end{aligned} \quad (\text{S16})$$

Thus j labels an j -channel process and the coupling amplitude is governed by Bessel functions. In typical experimental regimes the s - p bandwidth is small compared to their bare splitting, so only a single resonant j channel (usually $j = 1$ or $j = 2$) is relevant.

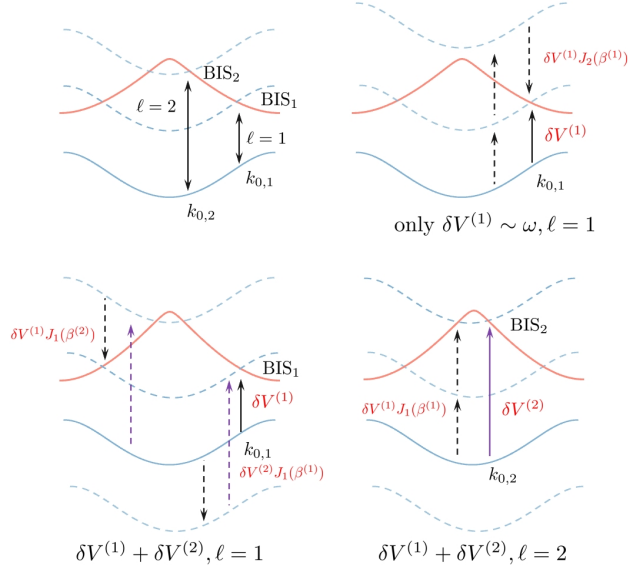


Fig. S1. Schematic illustration of the relevant resonant processes for single- and two-tone driving with multiple coherent channels. For two-tone driving, the single-photon resonance at the BIS₁ is addressed by the first-order process $\delta V^{(1)}$ at frequency ω_0 , as well as by second-order processes involving combinations such as $\delta V^{(1)} J_1(\beta^{(2)})$ and $\delta V^{(2)} J_1(\beta^{(1)})$. The two-photon resonance at BIS₂ is primarily driven by the first-order process $\delta V^{(2)}$ at $2\omega_0$, with additional contributions from higher-order processes involving $\delta V^{(1)}$.

For the one-photon resonant channel $j = 1$ Eq. (S16) reduces to

$$\begin{aligned}
 g_{-1}(k) &= \frac{d_y(k)}{2} \delta V^{(1)} [c_{-2}(k) + c_0(k)] \\
 &= \frac{d_y(k)}{2} \delta V^{(1)} \frac{2J_1(\beta^{(1)}(k))}{\beta^{(1)}(k)} \\
 &\approx \frac{d_y(k)}{2} \delta V^{(1)} \left[1 - \frac{\beta^{(1)}(k)^2}{8} \right] \equiv h_{F,y}(k),
 \end{aligned} \tag{S17}$$

where the expansion is valid for weak driving $|\beta^{(1)}| \ll 1$. The term $c_{-2}(k)$ originates from the time-periodic modulation of $d_z(k)$ and physically represents a higher-order (here, effectively third-order) process that nevertheless contributes to the single-photon resonance when combined with other harmonics. Retaining the $J_2(\beta^{(1)})$ contribution yields the estimate

$$\frac{d_y(k)}{2} \delta V^{(1)} c_{-2}(k) \simeq \frac{d_y(k) d_z(k)^2}{4\omega^2} (\delta V^{(1)})^3, \tag{S18}$$

consistent with a third-order amplitude scaling.

We now consider two-tone LDM with $j = 1, 2$. For the one-photon energy sector ($j = 1$) the off-diagonal coefficient can be written as

$$g_{-1}(k) = \frac{d_y(k)}{2} \left\{ \delta V^{(1)} [c_{-2}(k) + c_0(k)] + \delta V^{(2)} [e^{i\phi_2} c_{-3}(k) + e^{-i\phi_2} c_1(k)] \right\}, \tag{S19}$$

where we have taken the gauge $\phi_1 = 0$. For $\phi_2 = 0$ or π the coefficients remain real. Introducing the generalized Bessel combination

$$J_n(z_1, z_2; \phi) \equiv \sum_{m \in \mathbb{Z}} J_{n-2m}(z_1) J_m(z_2) e^{im\phi}, \tag{S20}$$

and keeping only the leading contributions in the small- β regime, one obtains the transparent approximation

$$\begin{aligned}
g_{-1}(k) &\approx \frac{d_y(k)}{2} [\delta V^{(1)}(c_0(k) + c_{-2}(k)) + \delta V^{(2)} e^{-i\phi_2} c_1(k)] \\
&= \frac{d_y(k)}{2} \delta V^{(1)} \left[J_0(\beta^{(1)}, \beta^{(2)}; \phi_2) + J_{-2}(\beta^{(1)}, \beta^{(2)}; \phi_2) \right] - \frac{d_y(k)}{2} \delta V^{(2)} e^{-i\phi_2} J_1(\beta^{(1)}, \beta^{(2)}; \phi_2) \\
&\approx \frac{d_y(k)}{2} \left\{ \delta V^{(1)} + e^{-i\phi_2} \left[\delta V^{(2)} J_1(\beta^{(1)}) - \delta V^{(1)} J_1(\beta^{(2)}) \right] \right\}, \tag{S21}
\end{aligned}$$

This expression shows explicitly that the second harmonic can coherently enhance or reduce the effective one-photon coupling depending on its amplitude and relative phase ϕ_2 . In the weak-driving limit ($\beta^{(j)} \ll 1$) the correction involving J_1 is small and one recovers $g_{-1}(k) \approx d_y(k) \delta V^{(1)}/2$, i.e. the single-frequency result.

For the one-photon channel ($j = 2$) and to the same order of approximation we obtain

$$\begin{aligned}
g_{-2}(k) &\approx \frac{d_y(k)}{2} [\delta V^{(1)} c_{-1}(k) + e^{-i\phi_2} \delta V^{(2)} c_0(k)] \\
&\approx \frac{d_y(k)}{2} [\delta V^{(2)} e^{-i\phi_2} - \delta V^{(1)} J_1(\beta^{(1)})]. \tag{S22}
\end{aligned}$$

The corresponding effective Floquet Hamiltonian on the $j = 2$ resonance is therefore

$$H_F^{(j=2)}(k) = [\Delta_z(k) - \omega] \sigma_z + [\Delta_0(k) - \omega] \sigma_0 + g_{-2}(k) \sigma_y. \tag{S23}$$

In summary, multi-tone LDM generates interference between different resonant channels. The relative phase ϕ_2 and the amplitudes $\delta V^{(1,2)}$ control both the magnitude and the sign of the effective transverse coupling fields $g_{-j}(k)$. This coherent control enables constructive or destructive combination of BIS contributions and can therefore invert the sign of the effective coupling field, which underlies the phase-tunable Floquet topological transitions reported in the main text. The retained formulae above show the origin and approximate size of the higher-order corrections that were omitted in the main text.

III. DETERMINING TOPOLOGY FROM BAND INVERSION SURFACES (BIS)

We first present the winding number of the Floquet bands as a function of the drive frequency, corresponding to the experimental results in Fig. 1(c) of the main text, as shown in Fig. S2. Throughout we set $\hbar = 1$, such that frequencies are expressed in energy units of E_r . The red dashed lines indicate the minimum ($\approx 3.5 E_r$ at $k = \pm\pi$) and maximum ($\approx 8.6 E_r$ at $k = 0$) energy differences $\Delta_{sp}(k) = E_p(k) - E_s(k)$ between the s and p bands for a static lattice with $V_0 = 3.5 E_r$. An interesting observation is that, for single-tone LDM, significant s - p coupling is observed only for $\omega_0 \gtrsim 4 E_r$, although the single-photon resonance condition would suggest an onset near $\Delta_{sp}^{\min} \approx 3.5 E_r$. This discrepancy may arise from two factors: (1) the quasimomentum distribution in the first Brillouin zone is typically non-uniform, with reduced population near the zone edges ($k = \pm\pi$), which suppresses the signal associated with $\Delta_{sp}(k \approx \pm\pi)$; (2) the Floquet-induced staggered s - p coupling has a k -dependent matrix element ($\propto \sin k$), further reducing contributions from $k = \pm\pi$. The observed high-frequency boundary is nevertheless consistent with $\Delta_{sp}^{\max} \approx 8.6 E_r$, which bounds the single-photon resonance window.

In contrast, for two-tone driving with ω_0 and $2\omega_0$, significant coupling is already observed when $2\omega_0 \approx 3.5 E_r$, likely because the off-resonant fundamental tone broadens the quasimomentum distribution and enhances the spectral weight of near-resonant states. When $2\omega_0 \approx 8 E_r$, the s - p coupling is strongly suppressed, which may result from destructive interference between the direct $2\omega_0$ channel and the effective second-harmonic component generated perturbatively by the ω_0 tone.

To theoretically analyze the topological invariants, we consider multi-frequency, even-time driving, which yields, for each resonant channel j , an effective Floquet Hamiltonian of the form

$$H_F^{(j)}(k) = \left[\Delta_z(k) - \frac{j\omega}{2} \right] \sigma_z + \Delta_0(k) \sigma_0 + g_{-j}(k) \sigma_y, \tag{S24}$$

where $g_{-j}(k)$ is the resonant off-diagonal coupling obtained from Eqs. (A11)-(A17). We note that both $j = 1, 2$ resonant channels correspond to one-photon processes, but the driving terms are more complex, involving contributions along both σ_z and σ_x axes, so care must be taken in analyzing the Hamiltonian.

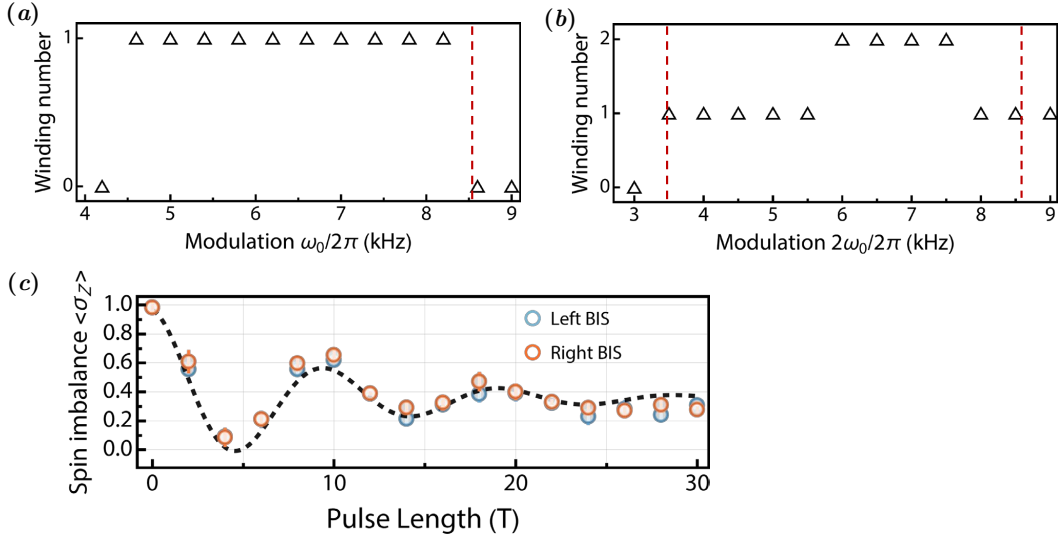


Fig. S2. (a,b) Winding number for Floquet bands with single-tone LDM at ω_0 and two-tone LDM at ω_0 and $2\omega_0$. Parameters are identical to those in Fig. 1(c) of the main text. (c) Typical oscillations between s and p orbitals for single-tone LDM in experiments. Parameters for (c): $V_0 = 4.3 E_r$, $\delta V_0 = 2 E_r$, and modulation frequency $\omega_0/2\pi = 8$ kHz.

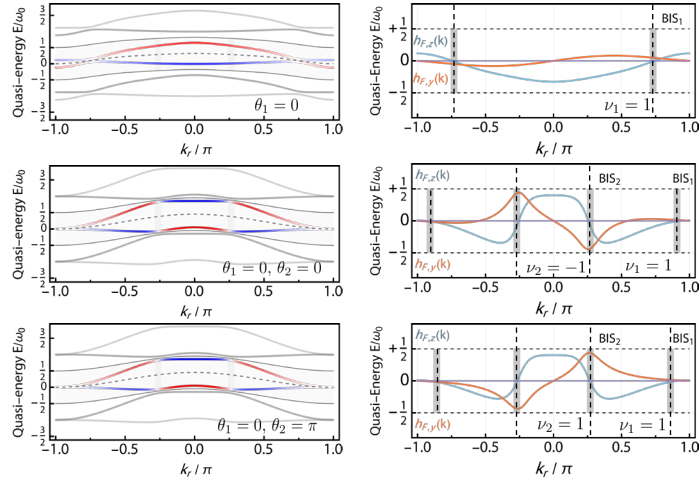


Fig. S3. Theoretically numerical results illustrating the identification of BIS momenta and their contributions to the winding number of the Floquet bands. Parameters are identical to those used in Fig. 1(d) of the main text.

For numerical calculations, we directly compute the stroboscopic Floquet generator as

$$U(T) = \mathcal{T} \exp \left[-i \int_0^T H(k, t) dt \right],$$

$$H_F(k) = \frac{i}{T} \log [U(T)], \quad (\text{S25})$$

where \mathcal{T} denotes time ordering. The components $h_{F,i}(k)$ are extracted from $H_F = \sum_i h_{F,i}(k) \sigma_i + h_{F,0}(k) \sigma_0$. Each drive-induced BIS is defined by the resonance condition for channel j :

$$h_{F,z}^{(j)}(k_{j,0}) = \Delta_z(k_{j,0}) - \frac{j\omega}{2} = 0. \quad (\text{S26})$$

For a BIS pair at momenta $k_{j,L}$ and $k_{j,R}$, we evaluate the transverse field $h_{F,y}(k)$ at these points and define the

topological invariant as

$$\nu_j = \frac{1}{2} [\text{sgn } h_{F,y}(k_{j,R}) - \text{sgn } h_{F,y}(k_{j,L})]. \quad (\text{S27})$$

We adopt the same gauge for both 0- and π -BIS to enable direct comparison within the Floquet Brillouin zone.

The gap-resolved winding numbers appearing in the main text are obtained by summing ν_j over BISs belonging to each gap:

$$W_0 = \sum_{j \in 0} \nu_j, \quad W_\pi = \sum_{j \in \pi} \nu_j, \quad (\text{S28})$$

and the total winding of the lowest Floquet band in our convention is $W = \sum_j (-1)^{\alpha_j/\pi} \nu_j$, equivalently reported as the pair (W_0, W_π) in the main text. Typical results are as follows: For single-tone LDM targeting the first resonant channel ($j = 1$), the BIS is located by $\Delta_z(k_0) - \omega/2 = 0$, and the numerically obtained sign pattern yields $\nu_1 = 1$, so $W_0 = 1$. For two-tone LDM, the two BIS pairs satisfy $\Delta_z(k_{j,0}) - j\omega/2 = 0$ for $j = 1, 2$. The relative phase of the second harmonic controls the sign of $g_{-2}(k)$ and thus the assignment of ν_j . Numerically, for $\phi_0^{(2)} = 0$: $\nu_1 = 1$ and $\nu_2 = 1$, so $W_0 = W_\pi = 1$ and the total invariant is $W = 2$. For $\phi_0^{(2)} = \pi$: $\nu_1 = 1$ and $\nu_2 = -1$, so $W_0 = 1$, $W_\pi = -1$, and $W = 0$.

These numerical values are obtained by evaluating $h_{F,y}(k_{j,L/R})$ from the computed $H_F(k)$ (using the same gauge for 0- and π -BIS) and applying Eq. (S27). The sign change of $h_{F,y}(k)$ between BIS pairs when the second-harmonic phase is flipped is the origin of the phase-tunable Floquet topological properties reported in the main text.

IV. GENERAL FORM FOR FLOQUET-RAMSEY MEASUREMENTS

In this section we derive a general expression for the two-pulse Ramsey signal for different shaking protocols. From the Bloch-rotation viewpoint, the mapping from an initial Bloch vector $\mathbf{n}_0(k)$ to the final vector $\mathbf{n}_f(k)$ produced by two pulses separated by a dark time τ_d can be written as

$$\mathbf{n}_f(k) = \hat{R}(\mathbf{n}_2, \Theta_2) \hat{R}(\mathbf{z}, \Theta_z) \hat{R}(\mathbf{n}_1, \Theta_1) \mathbf{n}_0(k), \quad (\text{S29})$$

where $\hat{R}(\mathbf{n}, \Theta)$ denotes rotation about axis \mathbf{n} by angle Θ , and $\Theta_i(k) = 2|\mathbf{h}_i(k)|t_i$ for the i -th pulse. The Rodrigues' rotation formula for arbitrary normalized vector \mathbf{n}_0 is

$$\hat{R}(\mathbf{n}, \Theta) \mathbf{n}_0 = \mathbf{n}_0 \cos \Theta + (\mathbf{n} \times \mathbf{n}_0) \sin \Theta + \mathbf{n}(\mathbf{n} \times \mathbf{n}_0)(1 - \cos \Theta), \quad (\text{S30})$$

and we projecting onto the z -axis yields the general interferometric form for initial state $\mathbf{n}_0 = (0, 0, -1)$ in the main text

$$n_{f,z}(k) = -[\mathcal{A}(k) + \mathcal{V}(k) \cos[\Phi(k) - \Phi_0(k)]], \quad (\text{S31})$$

with

$$\begin{aligned} \mathcal{A}(k) &= \prod_{i=1}^2 [c_i + (1 - c_i)(n_{i;z})^2], \\ \mathcal{C}(k) &= \prod_{i=1}^2 [n_{i;x} - (-1)^i i n_{i;y}] [(1 - c_i)n_{i;z} + (-1)^i i s_i], \\ \mathcal{V}(k) &= |\mathcal{C}(k)|, \quad \Phi_0(k) = \arg \mathcal{C}(k). \end{aligned} \quad (\text{S32})$$

Here $c_i = \cos \Theta_i$, $s_i = \sin \Theta_i$, and $\mathbf{n}_i(k) = \mathbf{h}_i(k)/|\mathbf{h}_i(k)|$ are the normalized rotation axes for pulses $i = 1, 2$. The dynamical phase accumulated during the dark interval is $\Phi(k) = 2h_{1;z}(k)\tau_d$ if the first-pulse frame is used as frame reference.

As a concrete example, take the first pulse to be a one-photon LPS resonance used to prepare BIS states. Its Floquet field is $\mathbf{h}_F^{(s)}(k)$ with components (see e.g. [33])

$$\begin{aligned} h_{F,x}^{(s)}(k) &= \mu_0^{sP} \cos \phi_s, \quad h_{F,y}^{(s)}(k) = \mu_0^{sP} \sin \phi_s, \\ h_{F,z}^{(s)}(k) &= \frac{1}{2} [\epsilon_p - \epsilon_s - \omega_s + 2(t_p - t_s) \cos k], \end{aligned} \quad (\text{S33})$$

where μ_0^{sP} is the site-shaking matrix element and ϕ_s the shaking phase. Note that the spin-independent term $h_{F,0}^{(s)}(k) = -(t_p + t_s) \cos k$ does not effect the rotation, hence we drop it in the above equations. The second pulse is taken to be the LDM readout described by $H_F^{(j)}(k) = \sum_i h_{F,i}^{(j)}(k) \sigma_i$. Using Eqs. (S32) one obtains the general Ramsey-phase expression for a LPS–LDM joint sequence:

$$\begin{aligned} \Phi_0(k) &= \Delta\phi(k) + \arg \left[(1 - c_2) \frac{h_{2;z}(k)}{|h_2(k)|} + \mathbf{i}s_2 \right] \\ &\quad - \arg \left[(1 - c_1) \frac{h_{1;z}(k)}{|h_1(k)|} + \mathbf{i}s_1 \right], \\ \Delta\phi(k) &= \alpha_1 - \alpha_2 + \omega_1 t_1 + (\epsilon_p - \epsilon_s) \tau_d, \end{aligned} \tag{S34}$$

where $\alpha_i = \arg[h_{i;x} + \mathbf{i}h_{i;y}]$ and ω_1 is the carrier frequency of the first pulse. The fringe contrast is

$$\begin{aligned} \mathcal{V}(k) &= \frac{|h_{F,\perp}^{(j)}(k) h_{F,\perp}^{(s)}(k)|}{|h_F^{(j)}(k) h_F^{(s)}(k)|} \sqrt{\left[(1 - c_2) \frac{h_{F,z}^{(j)}(k)}{|h_F^{(j)}(k)|} \right]^2 + s_2^2} \\ &\quad \times \sqrt{\left[(1 - c_1) \frac{h_{F,z}^{(s)}(k)}{|h_F^{(s)}(k)|} \right]^2 + s_1^2}, \end{aligned} \tag{S35}$$

with $h_{F,\perp} = \sqrt{h_{F,x}^2 + h_{F,y}^2}$. These expressions summarize the Ramsey response for the protocols used in this work and clarify the role of pulse angles, phases and BIS geometry in interpreting the measured fringes.